10-6-2010

Location and Mechanism of Very Long Period Tremor During the 2008 Eruption of Okmok Volcano from Interstation Arrival Times

Matthew M. Haney
Boise State University

 DOI: 10.1029/2010JB007440

Location and mechanism of very long period tremor during the 2008 eruption of Okmok Volcano from interstation arrival times

M. M. Haney[1,2]

Received 31 January 2010; revised 30 April 2010; accepted 1 June 2010; published 6 October 2010.

[1] We describe continuous, very long period (VLP) tremor that occurred during the 2008 eruption of Okmok Volcano, Alaska. Due to its low frequency content in band from the 0.2–0.4 Hz, the wave field of the VLP tremor is relatively free of path effects. From continuous recordings of the VLP tremor on 2 three-component broadband and 3 single-component short-period instruments, we devise a method to locate the epicenter of the tremor based on interstation arrival times computed with cross correlation. We find the epicenter since the vertical and radial components of the VLP tremor wave field are dominated by Rayleigh waves and the time shifts are related to lateral propagation. Over the 4 h period studied, this procedure yields a location NNW of Cone D, close to the new cone built over the course of the eruption. Similar analysis using the transverse horizontal components from the 2 three-component broadband instruments yields strong constraints on the source mechanism of the VLP tremor. We observe an anomalous interstation arrival time due to the existence of a nodal plane in the Love wave radiation pattern. The orientation of a compensated linear vector dipole (CLVD) source estimated from the transverse components closely aligns with the regional maximum horizontal stress direction. The depth of the CLVD source is constrained by matching the vertical components to the Rayleigh wave radiation pattern at all five stations. We find the VLP tremor source depth to be 2 km BSL, positioned between the magma chamber at Okmok (>3 km BSL) and the surface.

Citation: Haney, M. M. (2010), Location and mechanism of very long period tremor during the 2008 eruption of Okmok Volcano from interstation arrival times, *J. Geophys. Res.*, *115*, B00B05, doi:10.1029/2010JB007440.

1. Introduction

[2] Perhaps the most common type of volcano seismicity encountered during eruptions is a long-duration earthquake lasting from minutes to years known as volcanic tremor [*McNutt*, 1992; *McNutt*, 2005; *McNutt and Nishimura*, 2008]. Whereas other types of volcano seismicity, for example volcano-tectonic (VT) earthquakes, are related to stresses acting on the solid portion of the volcano, tremor is the direct result of fluid movement within the volcano. Knowledge of the source of volcanic tremor and any time-dependent change in its behavior therefore offers key information for understanding the evolution of an eruption and evaluating volcanic hazards. The main difficulty in tremor interpretation lies in its more or less continuous nature and the lack of clear phase arrivals, in contrast to VT earthquakes. As a result, location and characterization of tremor has been a subject of ongoing research in volcano seismology [*Benoit and McNutt*, 1997; *Wegler and Seidl*, 1997; *Battaglia and Aki*, 2003; *Takagi et al.*, 2006; *Lokmer et al.*, 2009].

[3] The two most popular approaches to tremor location involve either the use of small-aperture arrays [*Chouet et al.*, 1997] or fitting the decay of tremor amplitude with distance [*Battaglia and Aki*, 2003]. Whereas small-aperture arrays are able to use the phase information in the tremor wave field, the decay of tremor amplitude with distance does not use phase and, as a result, can be applied to sparse seismic networks, such as those commonly in place at volcanoes for the purpose of locating local VT earthquakes. Small-aperture arrays can exploit phase information since volcanic tremor is usually found in the frequency band from 0.5 to 10 Hz, with predominant frequencies from 1 to 3 Hz [*McNutt and Nishimura*, 2008]. Thus, over the small-aperture array, the tremor wave field is coherent and time delays between stations may be measured. In this paper, we extend the array concept and show that the wave field of unusually low frequency volcanic tremor (<0.5 Hz) is coherent over length scales approaching the aperture of a traditional "sparse" seismic network. We demonstrate that when such very long period (VLP) tremor exists, as it did during the 2008 eruption of Okmok Volcano in Alaska

[1]Alaska Volcano Observatory, U.S. Geological Survey Alaska Science Center, Anchorage, Alaska, USA.
[2]Now at Department of Geosciences, Boise State University, Boise, Idaho, USA.

0148-0227/10/2010JB007440

[*Larsen et al.*, 2009], tremor can be located and characterized with methods based on continuous seismic correlations using stations separated by over 10 km. These observations are significant since, outside of the study by *Sabra et al.* [2006], research on continuous seismic correlations at volcanoes has exclusively focused on nonvolcanic sources, e.g., the oceanic microseism [*Brenguier et al.*, 2007, 2008; *Masterlark et al.*, 2010]. In this work, we demonstrate that a similar methodology can be applied during times of volcanic activity, when tremor dominates the oceanic microseism.

[4] The most distinctive feature of Okmok Volcano, located on the northeast portion of Umnak Island, is its large (10 km diameter) caldera, the result of two caldera-forming eruptions in the past 12,000 years [*Finney et al.*, 2008]. Those two events represent a significant departure from the effusive basaltic style of eruptions typical at Okmok which are responsible for its broad shield. The caldera interrupts the shield structure, with the rim at 1 km in elevation and an average elevation of 400 m within the caldera. Okmok Volcano is one of the most active volcanic centers in the Aleutian Arc, averaging an eruption once every ten years during the 20th century. The eruptions during this time all originated from the southwest sector of the caldera, from an intracaldera cone known as Cone A. In fact, prior to 2008, the most recent eruption at Okmok from anywhere besides Cone A occurred in 1817, at Cone B [*Beget et al.*, 2008]. It is thought that the 1817 eruption at Cone B had a phreatomagmatic character similar to the 2008 eruption. The most recent eruption, prior to 2008, took place in 1997 and was associated with a roughly circular pattern of deformation about the center of the caldera [*Mann et al.*, 2002; *Miyagi et al.*, 2004; *Lu et al.*, 2005]. Due to its frequent activity, Okmok poses a threat to aviation in the heavily used north Pacific air traffic corridors. Moreover, the 2008 eruption of Okmok did not follow a long sequence of precursory seismic activity, reaching full eruption from background levels in less than 5 h, and it did not emanate from an established intracaldera cone, instead building a new cone to the NW of Cone D during the eruption [*Larsen et al.*, 2009].

[5] The 2008 eruption of Okmok Volcano lasted over a month during July and August, with VLP tremor persisting the entire time. VLP tremor in the frequency band from 0.2 to 0.5 Hz has been reported before at Stromboli [*De Lauro et al.*, 2005, 2006]. Periods as long as 12 s have been observed in the tremor wave field at Usu [*Yamamoto et al.*, 2002]. This low-frequency band is noteworthy in seismology due to its high level of ocean-generated microseismic noise. For this reason, the frequency band from 0.2 to 0.5 Hz has recently become the subject of interest for applications of ambient noise tomography at volcanoes [*Brenguier et al.*, 2007; *Masterlark et al.*, 2010]. Though notorious for ocean-generated noise, nothing precludes volcanoes from radiating energy within this band during eruptions, although it is apparently rare for volcanic tremor to be much lower than 0.5 Hz. We focus on the properties of VLP tremor produced during the 2008 Okmok eruption. The VLP tremor drowns out ocean-generated noise at these frequencies and motivates the development of analysis techniques based on the high degree of waveform similarity between stations.

[6] As pointed out by *Almendros and Chouet* [2003], several methods can measure waveform similarity, including cross correlation, coherence, and semblance. We compute time shifts and measure waveform similarity between pairs of traces at Okmok Volcano by finding the maximum cross-correlation value in small, running time windows. This same procedure is applied in the Doublet Method [*Poupinet et al.*, 1984; *Roberts et al.*, 1992; *Ratdomopurbo and Poupinet*, 1995] and Coda Wave Interferometry [*Snieder et al.*, 2002; *Snieder and Hagerty*, 2004; *Snieder*, 2006; *Wegler et al.*, 2006; *Haney et al.*, 2009] to repeating signals at the same station occurring at different times. In this study, we turn this procedure around and compute time shifts between different stations at the same time. Thus, instead of interevent time shifts, we analyze interstation time shifts. Interstation arrival times have recently been used within the framework of ambient noise correlation techniques to locate source regions of globally observed ocean-generated seismic noise of 26 s period [*Shapiro et al.*, 2006]. Although the method described by *Shapiro et al.* [2006] is similar in many ways to what we apply for volcanic tremor location, our method measures interstation phase arrival times instead of interstation group arrival times, a distinction which is important when the wave field is dominated by surface waves, as is the case typically for volcanic tremor. The use of continuous seismic correlations means the method has the potential to resolve time-dependent behavior of volcanic tremor, a property that has implications for volcano monitoring.

2. Data

[7] Within the network operated by the Alaska Volcano Observatory (AVO), spanning the entire Aleutian Arc, Okmok Volcano has the distinction of being the westernmost volcano with over 10 local stations and multiple broadband instruments. The local seismic network at Okmok Volcano is depicted in Figure 1. Also shown in Figure 1 are the locations of three intracaldera cones discussed in this study, Cones A, B, and D. Due to the extensive network, advanced seismic techniques can be applied at Okmok, for instance ambient noise tomography [*Masterlark et al.*, 2010]. Unfortunately, not all of the stations at Okmok are available to study the 2008 eruption seismicity. The stations within and close to the caldera (OKCD, OKCE, and OKER) sustained heavy damage during the initial explosive phase of the eruption. Other stations, such as OKCF, OKTU, and OKID, had operational issues that existed prior to and continued throughout the eruption.

[8] In this study, we use data from 3 short period (OKWR, OKWE, and OKRE) and 2 broadband stations (OKSO and OKFG). For reasons described later, we do not use data from the distant short-period stations OKSP and OKAK, although these stations successfully recorded data during the eruption. The short-period stations at Okmok are L4 Mark Products instruments with a sampling rate of 100 Hz; the broadbands are Guralp 6-TDs with 50 Hz sampling. All data within the Okmok network is transmitted in real time to AVO for the purpose of monitoring. Much is known about the complete system response for the two types of instruments, and accurate instrument corrections, taking into account the telemetry for the short-period instruments, can be applied to the recordings [*Masterlark et al.*, 2010].

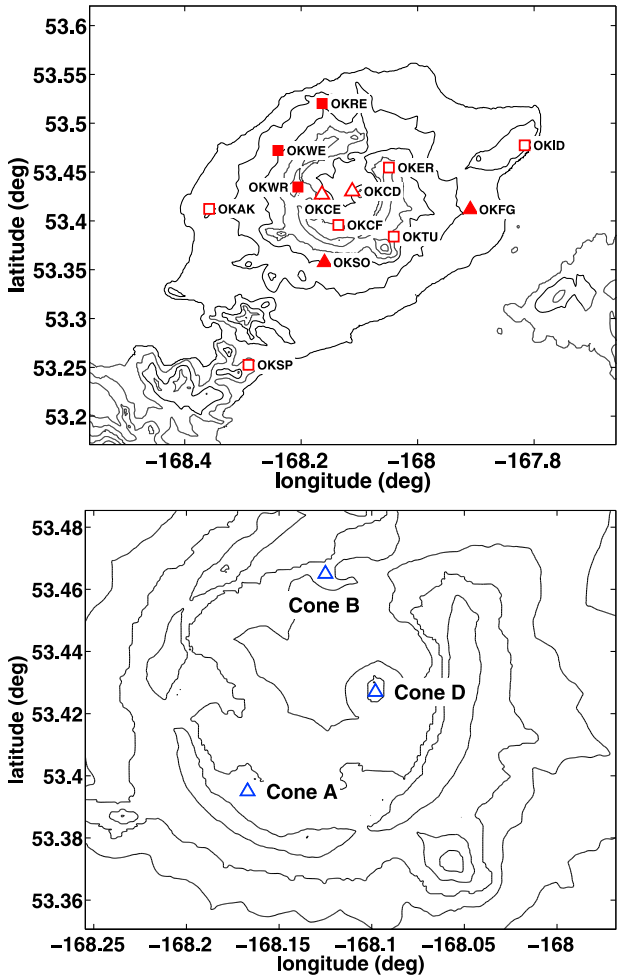

Figure 1. (top) The Okmok Volcano seismic network, composed of broadband (triangles) and short-period (squares) instruments. The stations used in this study are shown as filled shapes, whereas unused stations are unfilled. (bottom) Zoom of the caldera, showing the location of the three intracaldera cones discussed in the text (Cones A, B, and D).

Although the instruments recorded VLP tremor during the entire eruption, we limit the discussion here to 4 h of VLP tremor recorded between 1200 and 1600 UTC on 23 July 2008. The VLP tremor during these 4 h was typical of the majority of the VLP tremor over the entire monthlong eruption. Two exceptions, discussed briefly in a later section, were the VLP tremor during the initial explosive episode on 12 July and a period of strong tremor on 2 August.

[9] Shown in Figure 2 is a time series of Real-time Seismic Amplitude (RSAM) during the entire eruption and a helicorder plot of typical seismicity over a 24 h period on 28 July 2008. From the RSAM time series, tremor is observed to have persisted throughout the eruption, although its level waxed and waned. The seismicity in the helicorder plot is characterized by periods of continuous tremor interrupted by bursts of higher-amplitude low-frequency earthquakes [*Larsen et al.*, 2009]. This study focuses on the continuous tremor, as recorded on the 3 short period and 2 broadband seismometers surrounding the caldera (Figure 1). Clipping is an issue for the short-period stations at times of strong tremor and, as a result, we have concentrated the analysis on times of moderate tremor when the short-period stations were not saturated. We chose 4 h of tremor, which occurred between 1200 and 1600 UTC on 23 July 2008, to study due to its moderate strength and lack of clipping on the short-period instruments. Figure 3 shows the power spectrum of typical tremor on the vertical component of the broadband station OKFG along with background noise measured prior to the eruption. The tremor radiates a significant portion of its energy below 2 Hz, with some energy above the noise within the VLP band between 0.2 and 0.4 Hz. In spite of the low frequency, the short-period stations also record the VLP tremor. In fact, *Masterlark et al.* [2010] have previously demonstrated that the short-period stations at Okmok record the much weaker oceanic microseismic noise during times of quiescence over the same frequency band.

3. Interstation Arrival Times: Vertical Components

[10] Recent advances in seismology have highlighted the advantages of cross correlation applied to continuous seismic data [*Shapiro et al.*, 2006; *Brenguier et al.*, 2008]. We adopt this approach to investigate the source of VLP tremor at Okmok. The technique rests on the assumption that the waveforms in the VLP band at different stations are highly similar and differ mostly by a time delay. The time delay for a single station pair is the interstation arrival time. The radial semblance method [*Almendros and Chouet*, 2003] also exploits the similarity of waveforms in the VLP band; however, the radial semblance method is designed for the analysis of distinct VLP events whose wave field is composed of body waves. In contrast, the technique we describe is suited for continuous VLP tremor with a wave field made up of surface waves (Rayleigh or Love waves). The high similarity of the VLP tremor waveforms results from the low frequency content, since the long wavelengths do not sense spatially variable fine-grained structure in the subsurface. Waveforms in the VLP band are expected to be effectively free of path effects over the length scale of the volcano.

[11] A test of this hypothesis is presented in Figure 4. Shown are power spectra of the 2 broadband stations near 0.3 Hz for the 4 h period of continuous tremor between 1200 and 1600 UTC on 23 July 2008. The spectra are computed from recordings that have been instrument-corrected to particle velocity. Note that, although the broadband stations are 17 km apart, their power spectra are highly similar, with peaks and troughs lying nearly on top of each other. This observation supports the assumption that the main difference between the VLP tremor signals lies in the phase spectrum. In the cross-spectral technique [*Poupinet et al.*, 1984], a time delay between a signal pair is found from the linearity of the difference in their phase spectra. This approach can be improved considerably with the use of coherency-based filtering [*Rowe et al.*, 2002].

[12] Instead of the cross-spectral method, we turn to the time-windowed cross-correlation function between pairs of stations as employed in the technique known as Coda Wave Interferometry [*Snieder et al.*, 2002]. This procedure mar-

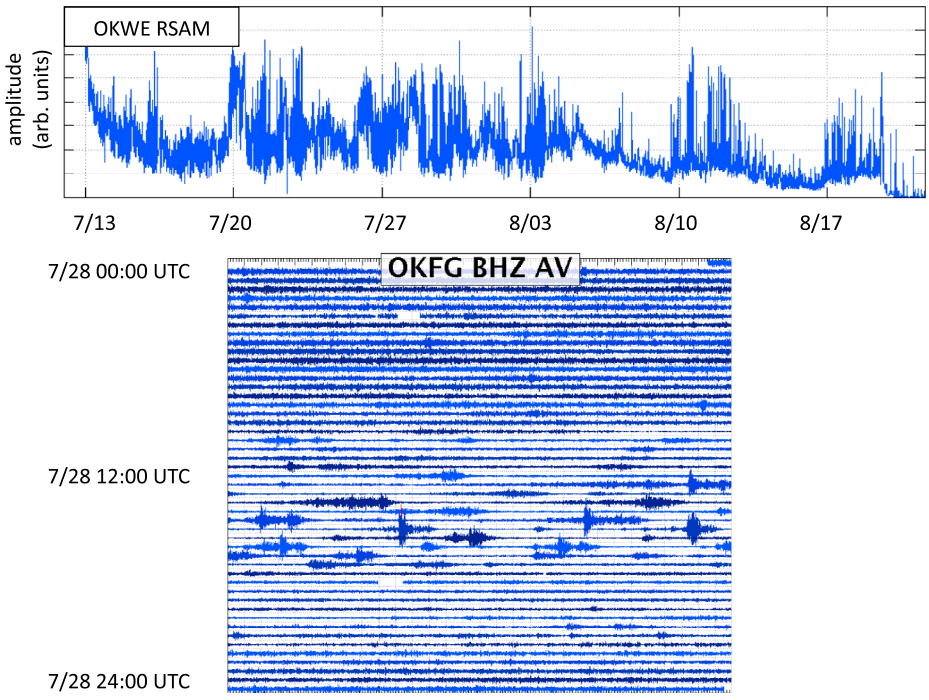

Figure 2. (top) Real-time seismic amplitude (RSAM) at station OKWE over the entire monthlong eruption. Moderate volcanic tremor occurred continuously during the eruption, with periods of stronger tremor interspersed. (bottom) A typical helicorder plot of seismicity over a 24 hour period during the 2008 eruption of Okmok. Hours of continuous tremor are seen to be interrupted by bursts of low-frequency events. Volcano seismicity dominates the entire helicorder plot, being substantially above the background noise level.

ches over all time samples in the 4 h time period and, at each sample, takes a small window from both data streams, cross-correlates them, and finds the time lag corresponding to the maximum correlation coefficient. Given two seismograms $u_A(t)$ and $u_B(t)$, the method therefore seeks the maximum of the following normalized cross-correlation function [*Snieder et al.*, 2002]

$$C(t,T,t_s) = \frac{\int_{t-T}^{t+T} u_A(t')u_B(t'+t_s)dt'}{\left(\int_{t-T}^{t+T} u_A^2(t')dt' \int_{t-T}^{t+T} u_B^2(t')dt'\right)^{1/2}}, \quad (1)$$

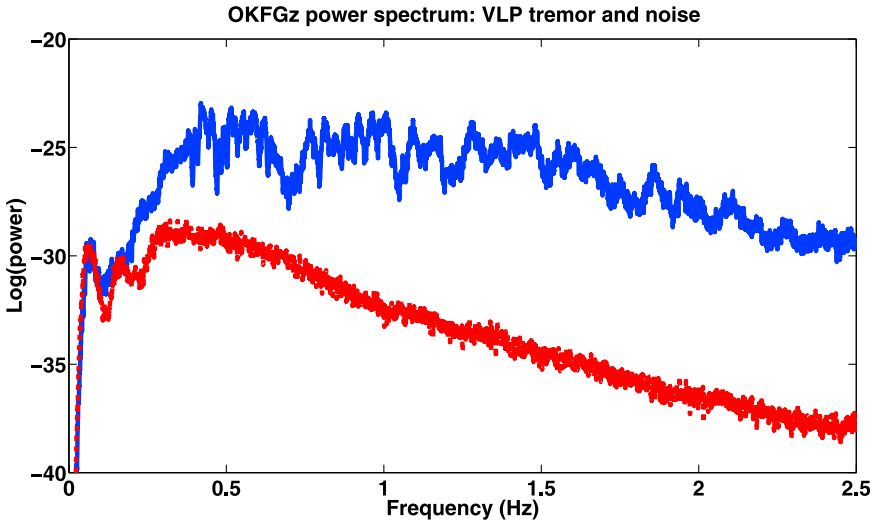

Figure 3. The power spectrum of the typical eruption tremor at Okmok compared with the power spectrum of background noise prior to the eruption. Significant tremor energy exists below 2 Hz, with a sizable portion above the noise within the VLP band from 0.2 to 0.4 Hz.

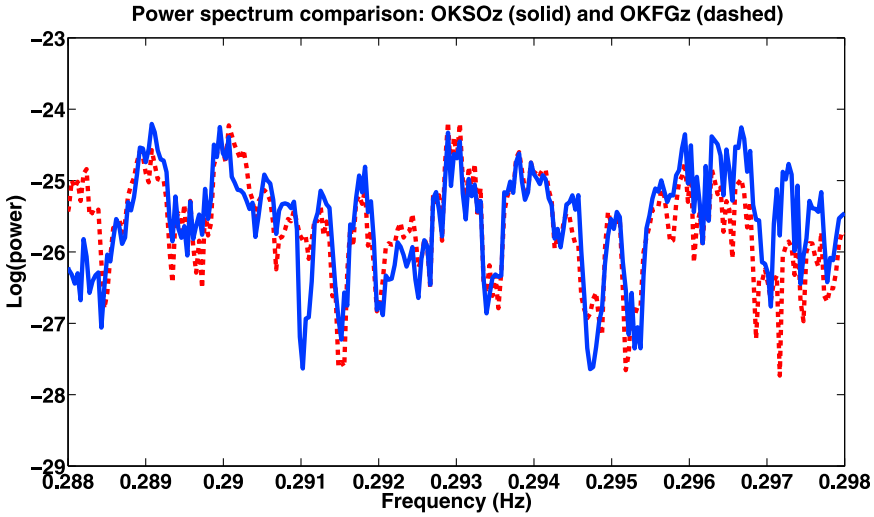

Figure 4. Zoom of the power spectra (computed with a multitaper method) near 0.3 Hz for the two broadband stations OKSO and OKFG at Okmok. Although the stations are 17 km apart, their power spectra are highly similar. This indicates that the main difference between the two signals lies in their phase spectra.

over all time samples t, where T is the half-length of the small time window taken from both data sets and t_s is the time lag. The time lag corresponding to the maximum value of C, given by $t_s^{\max}$, is a single estimate for the interstation arrival time for the station pair at time t given a half-window T. By applying this technique to 4 h of continuous tremor data, many thousands of estimates can be made and their statistics can be analyzed.

[13] Prior to forming the normalized cross-correlation function C, we instrument-correct and then bandpass the seismograms in the VLP tremor band of interest, between 0.2 and 0.4 Hz. After bandpassing with a third-order Butterworth filter, we decimate the short period and broadband data to a uniform sampling rate of 5 Hz. A sampling rate of 5 Hz is more than adequate to represent VLP tremor signals with frequencies between 0.2 and 0.4 Hz. The instrument-corrected, bandpassed, and decimated data from a single station pair is then analyzed using equation (1) and the time lag of the maximum correlation for each sample is saved over all times. For the time-windowed correlations, we use a half-window $T = 8$ s. Therefore, the entire window captures roughly 5 complete oscillations of the VLP tremor centered at 0.3 Hz. At each time sample, we only accept the computed time lag of the maximum correlation if the maximum correlation coefficient C has a value greater than 0.7 [*Wegler et al.*, 2006]. This makes the method robust in the presence of electronic noise by only saving time lags when the two signals are sufficiently similar to warrant doing so. This is similar to the coherency-based filtering technique described by *Rowe et al.* [2002].

[14] Figure 5 shows the interstation arrival times, or the time lags of the maximum correlation, as a function of time

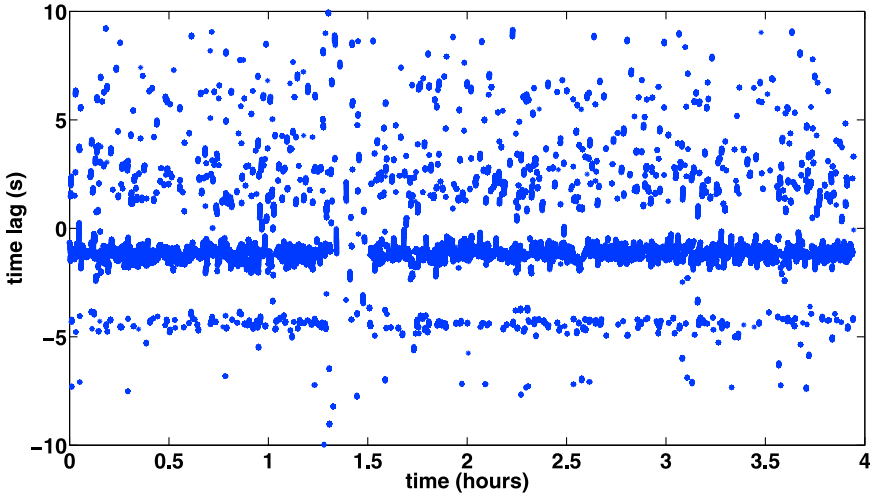

Figure 5. Raw interstation arrival times computed over the 4 h period between stations OKSO and OKFG. Note the dense clustering of the raw interstation arrival times around a time lag of −1 s. The weaker clustering around −5 s is related to cycle skipping in the cross correlation.

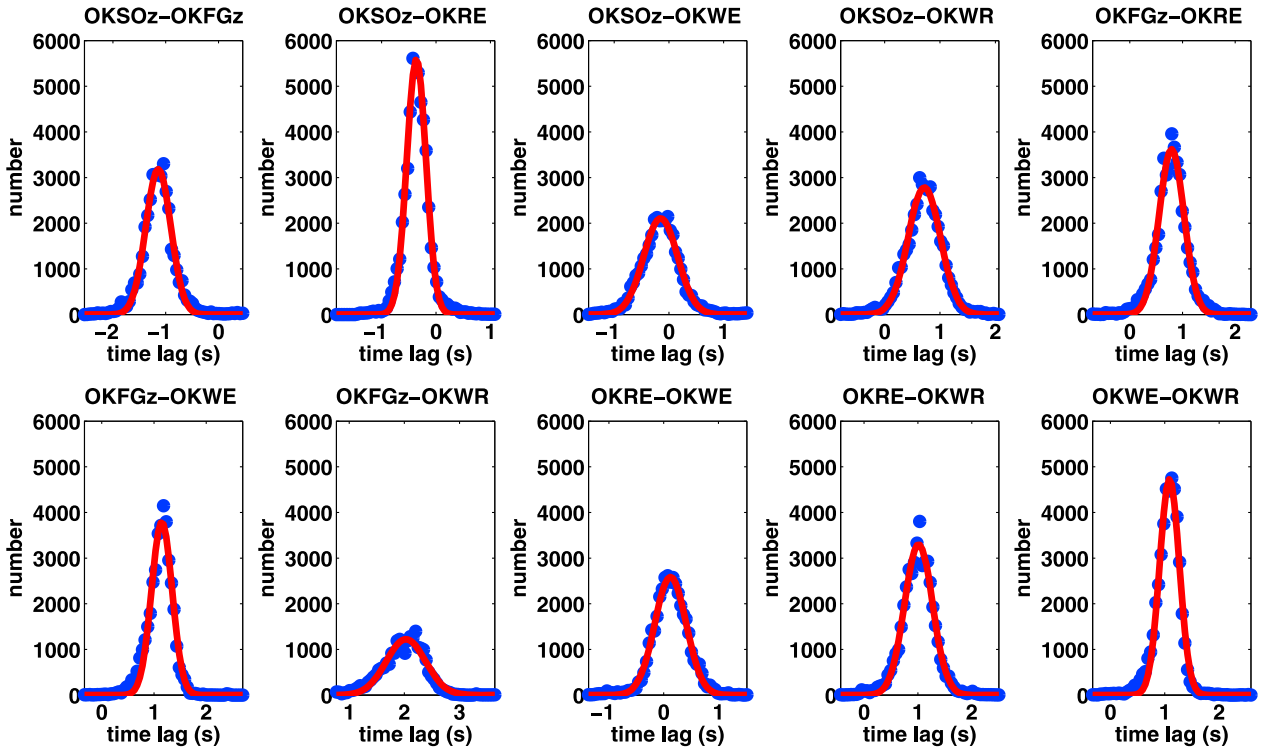

Figure 6. Four hour histograms of the raw interstation arrival times for all 10 pairs of vertical components at Okmok. The top left-hand plot corresponds to the histogram of the time lags in Figure 5. The histograms have been fit with Gaussian curves in order to estimate the dominant interstation arrival times and associated errors shown in Table 1.

over the 4 h studied for the station pair OKFGz and OKSOz. Although individual time lags vary between −10 s and 10 s, the majority of the time lags over the 4 h cluster about a time lag of roughly −1 s, forming a distinctive "streak." Some weaker clustering also occurs near a time lag of −5 s; it turns out that this weak clustering arises from cycle skipping. The presence of the dominant streak at a time lag of −1 s demonstrates that, although the VLP tremor is itself a random, continuous signal, the interstation arrival time between the station pair is more or less repeatable from time sample to time sample. Note that this streaking pattern is only observed for the VLP tremor and is absent for frequency bands higher than the band between 0.2 and 0.4 Hz. This is likely the result of path effects becoming important above 0.5 Hz, with a loss of coherence between stations arising from the associated path-dependent distortions of the waveforms.

[15] The average properties of the tremor over the 4 h period can be analyzed by binning the computed interstation arrival times and forming a histogram. The histogram associated with the station pair OKSOz-OKFGz is plotted as the blue dots in Figure 6 in the top left plot. One can observe that, indeed, the histogram is peaked at a time lag of approximately −1 s, corresponding to the main streak in Figure 5. Plotted along with the histogram in Figure 6 in the top left plot is a best fit Gaussian curve in red. The best fit Gaussian is found through nonlinear optimization using a Simplex algorithm with L2-norm minimization. From the best fit Gaussian, we can associate the time lag at the peak with the average interstation arrival time for the station pair. The width of the Gaussian gives an indication of the uncertainty in the value of the interstation arrival time.

[16] With a total of 5 vertical component recordings (3 short period and 2 broadband), the process we have described can be repeated for all 10 possible station pairs. The histograms for all 10 station pairs are plotted in Figure 6, along with their best fit Gaussians. Each station pair has a dominant peak in the histogram associated with its interstation arrival time. In Table 1, we show the computed interstation arrival times for all 10 vertical component station pairs, in addition to the standard deviations derived from the widths of the Gaussians. Also shown in Table 1 are 3 additional station pairs, OKSOr-OKFGr, OKSOt-OKFGt,

Table 1. Interstation Arrival Time Estimates From 1200 to 1600 UTC 23 July 2008

Station Pair	Arrival Time (s)	Standard Deviation (s)
OKSOz-OKFGz	−1.14	0.24
OKSOz-OKRE	−0.36	0.18
OKSOz-OKWE	−0.15	0.31
OKSOz-OKWR	0.72	0.29
OKFGz-OKRE	0.79	0.24
OKFGz-OKWE	1.15	0.20
OKFGz-OKWR	2.03	0.36
OKRE-OKWE	0.12	0.29
OKRE-OKWR	1.01	0.26
OKWE-OKWR	1.09	0.18
OKSOr-OKFGr	−1.03	0.20
OKSOt-OKFGt	0.37	0.24
OKSOt-OKFG(-t)	−1.10	0.21

Table 2. Okmok Layered Velocity Model

Layer	V_P[a] (km/s)	Depth of Layer Top (km)
1	3.83	surface
2	3.89	0
3	5.08	1
4	5.19	2
5	5.47	3
6	6.18	4
7	6.19	10
8	6.45	12
9	6.90	15
10	7.41	20
11	7.70	25
12	7.90	33
13	8.10	47
14	8.30	66

[a] $V_P/V_S = 1.78$.

and OKSOt-OKFG(-t), that involve horizontal components from the 2 broadband stations and are discussed in a later section.

4. Epicentral Location of VLP Tremor

[17] Since eruption tremor wave fields are most often composed of surface waves, of both Rayleigh and Love type [*McNutt and Nishimura*, 2008], we assume the VLP tremor we measure on the vertical component seismometers at Okmok is primarily composed of Rayleigh waves. Later, we discuss additional evidence that supports this assumption based on the analysis of the horizontal components from the broadband seismometers. We may therefore invert the measured interstation arrival times for the epicentral location of VLP tremor at Okmok. The epicentral location is found since the delay times of Rayleigh waves, and surface waves in general, reflect lateral propagation. This inversion procedure is similar in many ways to the location of the globally observed microseism with a period of 26 s by *Shapiro et al.* [2006]. The main difference is that *Shapiro et al.* [2006] applied a technique based on long-duration cross correlations and interstation arrival times related to group speed delay, instead of the phase speed delay we find by using time-windowed cross correlations.

[18] To locate the epicenter of the tremor, we must know the propagation velocity of the Rayleigh waves. From the 1-D layered model for Okmok discussed by *Masterlark et al.* [2010] and shown in Table 2, we compute the Rayleigh wave phase velocity over the frequency band of interest. We numerically model Rayleigh wave speed and mode shapes using the finite-element method of *Lysmer* [1970]. Figure 7 shows the frequency-dependent Rayleigh wave speed and, assuming a center frequency of 0.3 Hz for the VLP tremor band from 0.2 to 0.4 Hz, we find a Rayleigh wave speed $V_R = 2.7$ km/s for the VLP tremor.

[19] We locate the epicenter of the VLP tremor with a visual method and a proper inversion approach using least squares. For two stations A and B with an interstation arrival time Δt, we can plot the x and y points that satisfy the "double square root" equation

$$V_R \Delta t = \sqrt{(x - x_B)^2 + (y - y_B)^2} - \sqrt{(x - x_A)^2 + (y - y_A)^2}. \quad (2)$$

[20] To move between local Cartesian coordinates x and y and longitude and latitude, we adopt the method of *Richter* [1943]. This visual method plots a hyperbola-like line on a map of Okmok for each station pair. The line represents the locus of possible epicenters that yield the observed interstation arrival time Δt. By plotting all 10 lines associated with the computed interstation arrival times in Table 1, the epicenter of the tremor can be identified from the common intersection point of all 10 lines.

[21] A more quantitative method poses the VLP epicenter location problem in similar way to conventional earthquake location. A matrix kernel G can be derived that relates the lateral location of VLP tremor to the vector of observed interstation arrival times. For n stations, the inverse problem takes the form

$$G[x\ y]^T = \left[\Delta t_1 \Delta t_2 \cdots \Delta t_{n(n-1)/2}\right]^T, \quad (3)$$

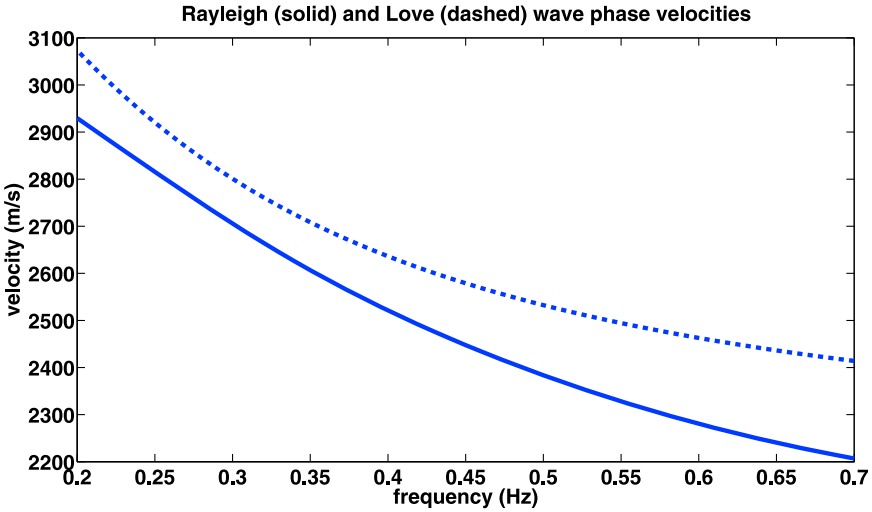

Figure 7. The Rayleigh and Love wave phase velocities for the Okmok velocity model in Table 2.

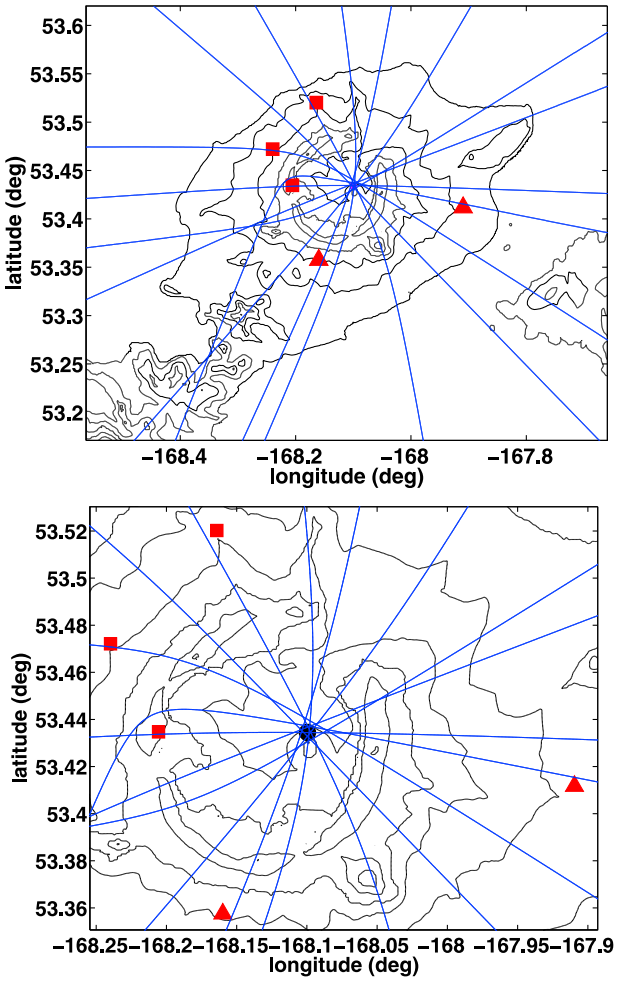

Figure 8. The epicentral location of the VLP tremor, (top) shown in relation to the entire northeast portion of Umnak island and (bottom) zoomed in to the caldera. The blue lines represent the loci of possible tremor locations for each of the 10 station pairs. The intersection of these blue lines indicates the location of the VLP tremor epicenter. The problem can also be solved using ordinary least squares, leading to the location given by the black dot.

where the model vector $\vec{m}$ is the lateral location (x and y or latitude and longitude) of the VLP tremor. Equation (3) can be solved with standard least squares.

[22] The results from both methods are plotted in Figure 8. Shown are the 10 hyperbola-like lines in blue and a black dot marking the result of the linearized inversion in equation (3). Many different initial guesses for the tremor location were used in the inversion and the final location was relatively insensitive to the initial guess. The final location from the inverse procedure (−168.1°W, 53.4°N) agrees closely with the common intersection of the 10 hyperbola-like lines. Therefore, the VLP tremor location is well constrained by the interstation arrival times. Figure 8 shows the epicenter location at the scale of the entire volcano and a zoom-in of the caldera area for clarity. Interestingly, we locate the epicenter of the tremor roughly 1 km to the NNW of Cone D, near to where the new cone was built during the 2008 eruption [*Larsen et al.*, 2009]. The proximity of the location to the new cone supports the interpretation of the VLP tremor as laterally propagating surface waves which experience simple time delay between the source and the stations at Okmok. The VLP tremor is therefore closely related to fluids and the venting of material at the new cone. The ability to locate the VLP tremor from 4 h of continuous recordings makes it possible to resolve changes in tremor location over the course of the monthlong eruption.

5. Interstation Arrival Times: Horizontal Components

[23] The epicentral location of the VLP tremor allows the analysis to go one step further by including the horizontal components from the 2 broadbands, OKSO and OKFG. The horizontal components can be rotated into radial and transverse components since the epicenter is known. For the VLP tremor, this means the Rayleigh and Love wave motions can be effectively separated, which is important since the two wave modes should be independent for an isotropic, elastic model of Okmok. Note that, as shown in Figure 7, the Love wave speed at 0.3 Hz (2.8 km/s) only slightly exceeds the Rayleigh wave phase speed (2.7 km/s). Thus, we may expect to find roughly the same interstation arrival time given Rayleigh or Love wave propagation.

[24] We apply the same sequence described previously to compute the histograms of the radial-radial and transverse-transverse correlations and find the associated interstation arrival times. Figure 9 (left) and 9 (middle) show the results for the radial pair OKSOr-OKFGr and the transverse pair OKSOt-OKFGt, respectively. The values of the interstation arrival times and the standard deviations for OKSOr-OKFGr and OKSOt-OKFGt are given in Table 1. The interstation arrival time for the radial pair, −1.03 s, agrees well with the earlier result for the vertical pair, −1.14 s. However, in contradiction to our expectation based on the similarity of Rayleigh and Love wave speeds, the interstation arrival time for the transverse pair, 0.37 s, is substantially different than the radial and vertical pairs.

[25] The substantially different value for the transverse pair can be understood by flipping the sign for one of the two transverse data channels. For instance, we flip the sign (i.e., multiply by −1) for the transverse component of OKFG and recompute the histogram of time lags. The recomputed histogram is shown in Figure 9 (right). As seen from the histogram, the sign flip causes the transverse pair to have an interstation arrival time, −1.10 s, that agrees with the radial and vertical pairs.

[26] We interpret the need for a sign flip to be an unequivocal indication for the existence of a nodal plane in the Love wave radiation pattern between stations OKSO and OKFG. Such information provides a strong constraint on the source mechanism of the VLP tremor at Okmok. We explore this in the following section and arrive at a model for a source mechanism that fits many of the VLP tremor observations. The difference we observe in the radial pair and transverse pair also provides evidence that our assumption of a tremor wave field composed of Rayleigh waves on the vertical and radial components and Love waves on the transverse component is well founded. Although we do not show the result here, the interstation arrival times computed from mixed radial-vertical correla-

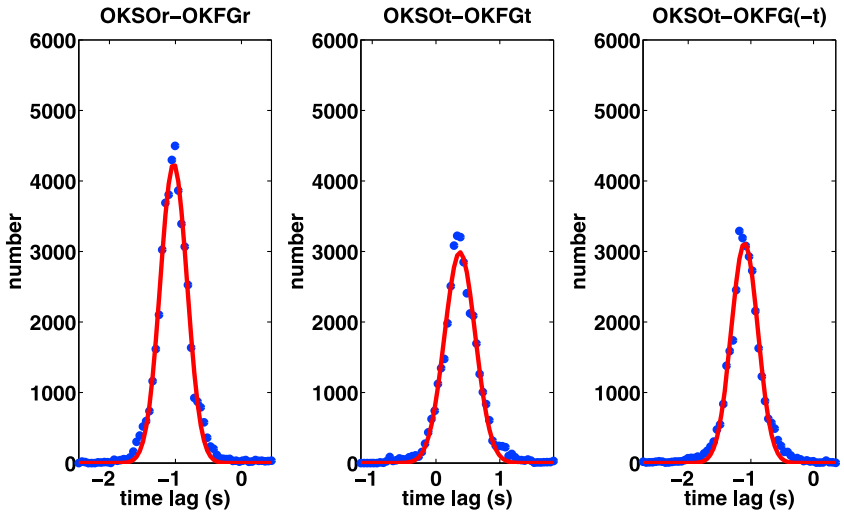

Figure 9. Four hour histograms from the (left) radial and (middle and right) transverse components at OKSO and OKFG. The interstation arrival time from the radial component agrees well with that computed from the vertical component. This is not the case for the transverse component (Figure 9, middle) unless one of the transverse components (in this case OKFG) is given a 180° phase shift (sign change). This key observation points to a nodal plane of Love wave radiation between OKSO and OKFG.

tions further supports the existence of Rayleigh waves since the delay times match closely with the delay time resulting from a $\pi/2$ phase shift at a frequency of 0.3 Hz.

6. Source Mechanism of VLP Tremor

[27] We attempt to reconcile our main observations with a model for the source mechanism of the VLP tremor. The two main observations are (1) the delay times computed from the vertical components yield an epicenter of the VLP tremor close to the location of the new cone built at Okmok during the 2008 eruption and (2) a nodal plane exists in the Love wave radiation pattern between stations OKSO and OKFG. A moment tensor that satisfies the first observation should not possess a significant, azimuth-dependent *initial phase* [*Muyzert and Snieder*, 1996]. An azimuth-dependent initial phase would imply that the interstation arrival times are not entirely related to time delays from propagation between the source and seismometer. There would be a relative source delay time associated with the difference in the initial phase for the different azimuths at the two stations. From the fact that we locate the epicenter close to the new cone without taking into account an initial phase, we conclude that the initial phase is negligible for the VLP tremor. The second observation, of a nodal plane in the Love wave radiation, requires a moment tensor that is not axially symmetric. The most simple model which satisfies these two observations is a moment tensor lacking the M_{xz} and M_{yz} components. We propose a physical model that leads to such a moment tensor and manually fit the predicted radiation pattern to observed instrument-corrected amplitudes.

[28] The subsurface structure at Okmok is known to consist of a shallow magma reservoir (>3 km BSL) more or less centered beneath the caldera [*Masterlark et al.*, 2010]. Therefore, a possible model for the source of the VLP tremor is a contracting spherical magma reservoir emptying into an arbitrarily oriented vertical dike or crack-like conduit. The moment tensor for flow into an arbitrarily oriented vertical dike follows from tensor rotation of a dike oriented with the coordinate system as [*Chouet*, 1996]

$$M_D(\theta) = \Delta V \begin{bmatrix} \cos\theta & \sin\theta & 0 \\ -\sin\theta & \cos\theta & 0 \\ 0 & 0 & 1 \end{bmatrix} \begin{bmatrix} \lambda+2\mu & 0 & 0 \\ 0 & \lambda & 0 \\ 0 & 0 & \lambda \end{bmatrix} \cdot \begin{bmatrix} \cos\theta & -\sin\theta & 0 \\ \sin\theta & \cos\theta & 0 \\ 0 & 0 & 1 \end{bmatrix}, \quad (4)$$

where θ is the azimuth of the long horizontal dimension of the crack or dike in degrees clockwise from north, λ and μ are the elastic Láme parameters, and ΔV is the volume of inflation due to flow into the vertical crack. Note that $\theta = 0°$ is a crack or dike oriented in the north-south direction. The moment tensor for flow out of a spherical magma reservoir is simply [*Chouet*, 1996]

$$M_S = -\Delta V \begin{bmatrix} \lambda+2\mu/3 & 0 & 0 \\ 0 & \lambda+2\mu/3 & 0 \\ 0 & 0 & \lambda+2\mu/3 \end{bmatrix}. \quad (5)$$

[29] When added together, the dike and chamber combine to form a compensated linear vector dipole (CLVD) source that satisfies conservation of mass

$$M = M_D(\theta) + M_S = \Delta V \mu \begin{bmatrix} 2\cos^2\theta - 2/3 & -2\sin\theta\cos\theta & 0 \\ -2\sin\theta\cos\theta & 2\sin^2\theta - 2/3 & 0 \\ 0 & 0 & -2/3 \end{bmatrix}. \quad (6)$$

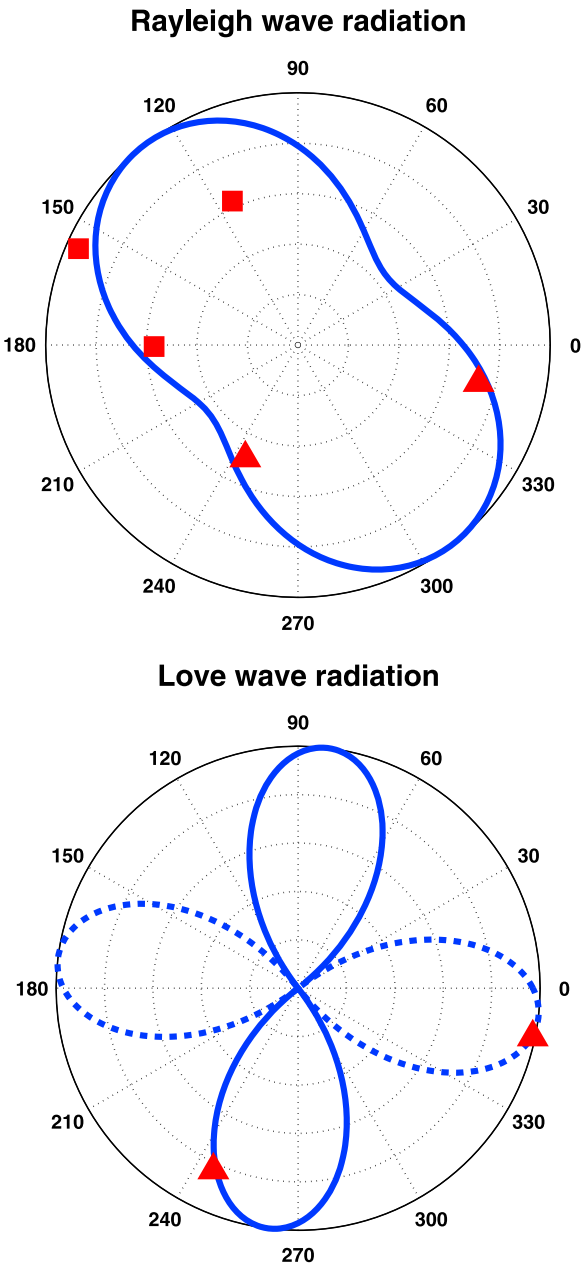

Figure 10. Rayleigh and Love wave radiation patterns at 0.3 Hz for the model of VLP tremor. Also shown are the average (top) vertical amplitudes and (bottom) transverse amplitudes for the two broadband stations (red triangles) and three short period stations (red squares). Stations OKSO and OKFG exist on two different lobes of the Love wave radiation, which differ in sign as shown by the solid and dashed parts of the Love wave radiation.

[30] Note that, consistent with our earlier discussion, this moment tensor lacks the M_{xz} and M_{yz} components. Thus, it is able to satisfy both of our main observations of VLP tremor at Okmok. We seek to refine this model by scanning over azimuth and depth of a source described by this moment tensor to see which one best fits the observed seismic radiation. It is worthwhile to point out that other source mechanisms may satisfy both of our main observations. One interesting candidate is a contracting horizontal sill emptying into an arbitrarily oriented vertical dike. This source also leads to a CLVD, although one with a slightly different form than equation (6). We return to this model in the discussion section. A single vertical dike, without an associated magma chamber or horizontal sill, satisfies both of the observations but, as described later, cannot be reconciled with the Rayleigh wave radiation pattern observed for VLP tremor at Okmok. In addition, a single vertical dike is not a CLVD and does not satisfy mass conservation.

[31] The azimuth of the vertical crack-like conduit can be found from the amplitude ratio R of the transverse components between two stations and their azimuths from the epicenter. From the expression for the far-field Love wave portion of the Green's function in the work of *Aki and Richards* [1980], we arrive the following expression relating the ratio of transverse amplitudes measured at two stations R, the azimuths from the source epicenter at the two stations ψ_1 and ψ_2, and the azimuth of the vertical crack orientation θ

$$\tan 2\theta = \frac{R\sin 2\psi_1 - \sin 2\psi_2}{\cos 2\psi_2 - R\cos 2\psi_1}. \tag{7}$$

[32] Note that the radiation pattern of the Love waves does not depend on the depth of the VLP tremor, in contrast to the Rayleigh wave radiation pattern. We find an amplitude ratio between the OKSO and OKFG transverse components of -0.84 ± 0.15 by averaging the value of the envelope at each station over the 4 h period and taking into account the sign difference between the stations. Prior to averaging the envelope, we apply instrument corrections and an inverse geometrical spreading factor for surface waves. From the value for the ratio R and the azimuths to OKSO and OKFG, we find that the azimuth of the long horizontal dimension of the vertical crack is 37° counterclockwise from north, so that the crack is oriented in the NW-SE direction. Figure 10 (bottom) shows the obtained Love wave radiation pattern at 0.3 Hz and the average transverse amplitudes at the two broadband stations. Stations OKSO and OKFG clearly exist on two different lobes of the Love wave radiation, which differ in sign as shown by the solid and dashed lines.

[33] The radiation pattern for Rayleigh waves differs from the Love waves in that it depends strongly on depth. This allows the depth of the VLP tremor to be constrained since we have obtained the azimuth of the vertical crack from the Love waves. In Figure 11, we show the Rayleigh wave radiation pattern at several depths, based on the expressions for the far-field Rayleigh wave portion of the Green's function in the work of *Aki and Richards* [1980]. Note how the radiation pattern consists of many lobes at shallow depths and depends strongly on depth for depths above 2.4 km. The transition in the radiation pattern from NE-SW oriented lobes at 1.2 km depth to NW-SE at 3.2 km depth is primarily controlled by the zero-crossing in the horizontal mode shape for the Rayleigh waves, as plotted in Figure 11 (bottom left). The isotropic radiation pattern at 2 km depth coincides with the zero-crossing of the horizontal component.

[34] By comparing the Rayleigh wave radiation patterns at different depths with the observed vertical component

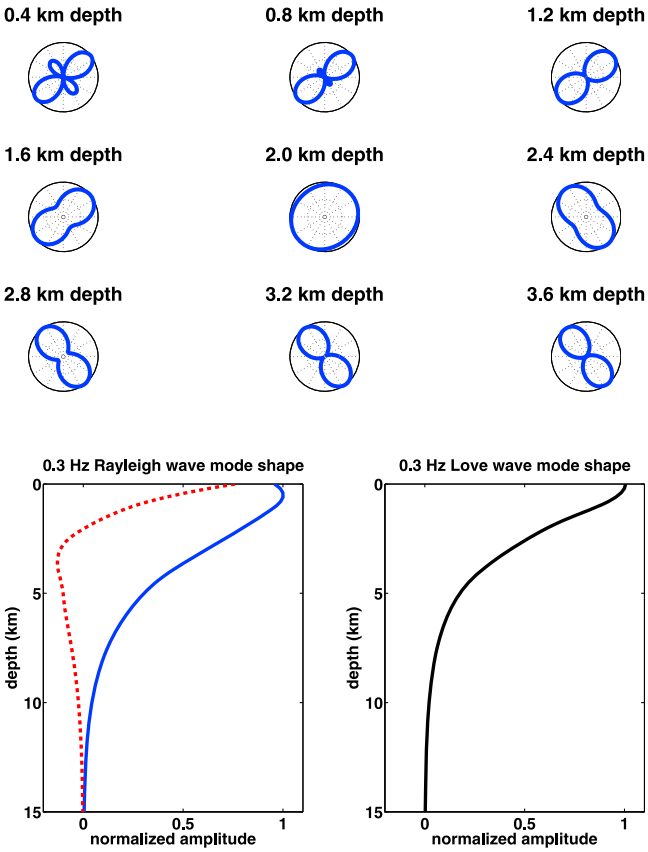

Figure 11. (top) Rayleigh wave radiation patterns as a function of source depth, showing the strong dependence of the radiation pattern at shallow (<2 km) depths. (bottom) The Rayleigh and Love wave mode shapes at 0.3 Hz. For the Rayleigh wave, the horizontal mode shape is shown as a dashed red line. The main factor controlling the Rayleigh wave radiation pattern is the zero crossing of the horizontal motion at approximately 2 km depth.

amplitudes, we can estimate the depth of the VLP tremor. Proceeding in the same way as in the analysis of the transverse components, we average the value of the envelope for the 5 available vertical components over the 4 h period, after accounting for instrument corrections and geometrical spreading. These are plotted in Figure 10 (top) along with the Rayleigh wave radiation pattern corresponding to a depth of 2.4 km. We find that the radiation pattern at 2.4 km depth best matches the observed averaged vertical component amplitudes. In fact, the match is striking except for the amplitude at the northernmost station, OKRE. The amplitudes at the 4 other stations more or less fall along the modeled radiation pattern. This may be the result of an anomalous site effect at OKRE or an error in the instrument specifications. Note that the radiation pattern at 2.4 km depth matches the data because it does not have any lobes or nodal planes and it predicts higher amplitudes in the NW-SE direction. Since the elevation of the caldera floor at Okmok is approximately 0.4 km above sea level, the VLP tremor source is located at a depth of approximately 2 km BSL. In our model, this depth corresponds to the junction of the vertical crack-like conduit with the spherical magma reservoir. Since the wavelengths of the VLP tremor are on the order of 8 km, the composite model of a vertical crack-like conduit and a spherical magma reservoir is treated as a point moment source [*Chouet*, 1996]. Regarding other possible source models, a horizontal sill emptying into a vertical dike can also explain the observed Rayleigh wave radiation pattern; however, the source depth in this case is deeper (3 km BSL) than the source model described above. In contrast, the Rayleigh wave radiation pattern from a single vertical dike cannot be reconciled with the observations, since it predicts higher amplitudes in the NE-SW direction.

7. Discussion

[35] The preferred model for the VLP tremor source mechanism agrees with regional models of Okmok Volcano known from other studies. For instance, the orientation of the vertical crack-like conduit, 37° counterclockwise from north, aligns nicely with the direction of regional maximum horizontal stress, as shown by *Johnson et al.* [2010]. The regional maximum horizontal stress direction is determined in large part by the local angle of plate convergence along the Aleutian Arc. This means that, above the shallow magma reservoir at Okmok, the main perturbation to the regional stress field due to the volcano is in the vertical direction; the horizontal stress field is largely unperturbed above the magma reservoir. *Johnson et al.* [2010] have discussed this issue in relation to their results on shear wave splitting direction at Okmok. It therefore appears the 2008 eruption of Okmok was fed by a vertical crack-like conduit aligned in the direction of regional maximum horizontal stress. Crack-like conduits at volcanoes have been observed previously, for instance at Aso Volcano in Japan [*Yamamoto et al.*, 1999]. In addition, the depth of the VLP tremor source, 2 km BSL, sits above the shallow magma reservoir, whose depth is known from recent seismic tomography results [*Masterlark et al.*, 2010] to be approximately 4 km BSL. The source depth therefore points to the VLP tremor arising from the transport of fluids out of the magma reservoir and toward the surface. It is worth pointing out that the crack-like conduit detected at Aso Volcano was found to exist at a similar depth of 1.8 km [*Yamamoto et al.*, 1999].

[36] In this study, we do not address the physical dimensions of the vertical crack at Okmok. However, we can make some qualitative statements about the size of the crack. The VLP tremor we analyze has wavelengths on the order of 8 km. Since we are able to explain several of the observations with a model of a seismic moment acting at a point in the subsurface, the vertical crack must be significantly smaller than the wavelength of the VLP tremor. A likely dimension for the crack would be on the order of 1 km; this is, for instance, the dimension found by *Yamamoto et al.* [1999] for the crack-like conduit at Aso Volcano. Finding the dimensions of the vertical crack at Okmok Volcano would require full-waveform numerical modeling and inversion, which is beyond the scope of this study. A subsurface structural model for such full-waveform methods could be drawn from the recent result of 3D ambient noise tomography at Okmok [*Masterlark et al.*, 2010]. A future application of waveform inversion to the VLP tremor wave field at Okmok can benefit from the results of this study since the preferred model we arrive at can be used as an initial model in the inversion.

[37] For our analysis, we utilize 3 short period and 2 broadband seismometers. Two other short period seismometers, OKAK and OKSP, exist at Okmok on the western side of the volcano (see Figure 1). We have attempted to use these in our analysis, but found that there is no coherence between these stations and the other stations. In other words, there is no "streaking" in the associated plot of time lags as in Figure 5. Since the VLP tremor was strong enough to register on OKAK and OKSP with a signal-to-noise ratio of approximately 5, the lack of coherence at stations OKAK and OKSP gives an indication of the maximum length scales over which waveform similarity is lost due to path effects in the subsurface for the VLP band. This points to substantial structural heterogeneity on the western side of the volcano.

[38] Although VLP tremor in the frequency band from 0.2 to 0.4 Hz existed over the course of the entire eruption, we have focused on 4 h of "typical" VLP tremor. By typical, we mean that most of the tremor analyzed during the entire eruption showed the same properties as the tremor highlighted here. There are two notable exceptions, however. During the initial explosive phase of the eruption on 12 July time-lag plots, such as the one in Figure 5, do not show streaking which is as pronounced as later in the eruption. We interpret this to mean that the vertical crack-like conduit was still forming during the initial explosive phase and did not acquire a stable structure until later in the eruption. In addition to this departure from typical tremor, an hour-long episode of intense VLP tremor that occurred on 2 August had unusual properties. Unfortunately, the intense tremor on 2 August clipped on the 3 short-period stations and, as a result, the epicenter of the tremor cannot be located. However, the recordings on the 2 broadbands did not clip, and the pattern of streaking in the associated time-lag plot for the pair of broadbands changed from its typical pattern during the period of intense tremor. The intense tremor of 2 August, therefore, had a different interstation arrival time between the two broadband stations. This observation points to the possible movement of the VLP tremor source during this time. Beyond these two tremor episodes, the initial explosive phase and the intense tremor on 2 August, the VLP tremor displayed stability over the course of the eruption.

8. Conclusions

[39] Based on cross correlations of continuous seismic data, we have estimated the epicentral location and depth of VLP tremor observed during the 2008 eruption of Okmok Volcano. The wave field of the VLP tremor consists mainly of surface waves, of both Rayleigh and Love type. Therefore, the location of the VLP tremor is a similar problem to the location of a tectonic earthquake from surface waves alone. The primary difference is that the waveform for the VLP tremor is continuous and random, whereas a tectonic earthquake has a compact and deterministic waveform related to its rupture. From interstation arrival times, we locate the epicenter of the VLP tremor to the NNW of Cone D, where the new cone was built during the 2008 eruption. The epicentral location of the VLP tremor at Okmok benefitted from the excellent azimuthal coverage of stations around the caldera. The critical observation leading to the estimate of the VLP tremor source mechanism depended on the existence of a pair of three-component broadband stations at Okmok, making it possible to observe the transverse components. We arrive at a model for the VLP tremor of a vertical crack-like conduit connected to a spherical magma reservoir. The vertical crack is oriented in the NW-SE direction (37° counterclockwise from north), in the direction of the maximum regional horizontal stress. We find the depth of the VLP tremor, where the vertical crack and the spherical magma reservoir connect, to be approximately 2 km BSL. Such a depth places the VLP tremor source between the caldera floor and the shallow (>3 km BSL) magma reservoir at Okmok. The VLP tremor represents the continuous flow of mass from the magma reservoir to the surface. This work demonstrates that, when VLP tremor exists, methods based on waveform similarity and continuous seismic correlations can be applied to stations from a traditional "sparse" seismic network to locate the tremor source, a longstanding problem in the field of volcano seismology.

[40] **Acknowledgments.** We thank Stephanie Prejean and John Power of the USGS Alaska Volcano Observatory for comments and discussions on Okmok Volcano. This work was partially funded under the USGS Mendenhall postdoctoral program and USGS/ARRA award G10AC00016.

References

Aki, K., and P. G. Richards (1980), *Quantitative Seismology*, W. H. Freeman, New York.

Almendros, J., and B. Chouet (2003), Performance of the radial semblance method for the location of very long period volcanic signals, *Bull. Seismol. Soc. Am.*, *93*(5), 1890–1903.

Battaglia, J., and K. Aki (2003), Location of seismic events and eruptive fissures on the Piton de la Fournaise volcano using seismic amplitudes, *J. Geophys. Res.*, *108*(B8), 2364, doi:10.1029/2002JB002193.

Beget, J., L. Almberg, J. Faust-Larsen, and C. Neal (2008), Eruption history of Cone D: Implications for current and future activity at Okmok Caldera, *Eos Trans. AGU*, *88*(52), Fall Meet. Suppl., Abstract A53B-0255.

Benoit, J. P., and S. R. McNutt (1997), New constraints on source processes of volcanic tremor at Arenal Volcano, Costa Rica, using broadband seismic data, *Geophys. Res. Lett.*, *24*(4), 449–452, doi:10.1029/97GL00179.

Brenguier, F., N. M. Shapiro, M. Campillo, A. Nercessian, and V. Ferrazzini (2007), 3-D surface wave tomography of the Piton de la Fournaise volcano using seismic noise correlations, *Geophys. Res. Lett.*, *34*, L02305, doi:10.1029/2006GL028586.

Brenguier, F., N. M. Shapiro, M. Campillo, V. Ferrazzini, Z. Duputel, O. Coutant, and A. Nercessian (2008), Toward forecasting eruptions using seismic noise, *Nat. Geosci.*, *1*, 126–130.

Chouet, B. (1996), New methods and future trends in seismological volcano monitoring, in *Monitoring and Mitigation of Volcano Hazards*, edited by R. Scarpa and R. I. Tilling, pp. 23–97, Springer, New York.

Chouet, B., G. Saccorotti, M. Martini, P. Dawson, G. De Luca, G. Milana, and R. Scarpa (1997), Source and path effects in the wave fields of tremor and explosions at Stromboli Volcano, Italy, *J. Geophys. Res.*, *102*(B7), 15,129–15,150, doi:10.1029/97JB00953.

De Lauro, E., S. De Martino, M. Falanga, M. Palo, and R. Scarpa (2005), Evidence of VLP volcanic tremor in the band [0.2–0.5] Hz at Stromboli volcano, Italy, *Geophys. Res. Lett.*, *32*, L17303, doi:10.1029/2005GL023466.

De Lauro, E., S. De Martino, M. Falanga, and M. Palo (2006), Statistical analysis of Stromboli VLP tremor in the band [0.1–0.5] Hz: Some consequences for vibrating structures, *Nonlinear Proc. Geophys.*, *13*, 393–400.

Finney, B., S. Turner, C. Hawkesworth, J. Larsen, C. Nye, R. Grorge, I. Bindeman, and J. Eichelberger (2008), Magmatic differentiation at an island-arc caldera: Okmok Volcano, Aleutian islands, Alaska, *J. Petrol.*, *49*, 857–884.

Haney, M. M., K. van Wijk, L. A. Preston, and D. F. Aldridge (2009), Observation and modeling of source effects in coda wave interferometry at Pavlof Volcano, *Leading Edge*, *28*, 554–560.

Johnson, J. H., S. Prejean, M. K. Savage, and J. Townend (2010), Repeating earthquakes, anisotropy and seismicity associated with the 2008 eruption of Okmok Volcano, Alaska, *J. Geophys. Res.*, *115*, B00B04, doi:10.1029/2009JB006991.

Larsen, J., C. Neal, P. Webley, J. Freymueller, M. Haney, S. McNutt, D. Schneider, S. Prejean, J. Schaeffer, and R. Wessels (2009), Eruption of Alaska Volcano breaks historic pattern, *Eos Trans. AGU*, *90*(20), 173–174.

Lokmer, I., G. S. O'Brien, D. Stich, and C. J. Bean (2009), Time reversal imaging of synthetic volcanic tremor sources, *Geophys. Res. Lett.*, *36*, L12308, doi:10.1029/2009GL038178.

Lu, Z., T. Masterlark, and D. Dzurisin (2005), Interferometric synthetic aperture study of Okmok Volcano, Alaska: Magma supply dynamics and postemplacement lava flow deformation, *J. Geophys. Res.*, *110*, B02403, doi:10.1029/2004JB003148.

Lysmer, J. (1970), Lumped mass method for Rayleigh waves, *Bull. Seismol. Soc. Am.*, *60*, 89–104.

Mann, D., J. Freymueller, and Z. Lu (2002), Deformation associated with the 1997 eruption of Okmok Volcano, Alaska, *J. Geophys. Res.*, *107*(B4), 2072, doi:10.1029/2001JB000163.

Masterlark, T., M. Haney, H. Dickinson, T. Fournier, and C. Searcy (2010), Rheologic and structural controls on the deformation of Okmok volcano, Alaska: FEMs, InSAR, and ambient noise tomography, *J. Geophys. Res.*, *115*, B02409, doi:10.1029/2009JB006324.

McNutt, S. R. (1992), Volcanic tremor, in *Encyclopedia of Earth System Science*, vol. 4, edited by W. A. Nierenberg, pp. 417–425, Academic, San Diego, Calif.

McNutt, S. R. (2005), Volcanic Seismology, *Annu. Rev. Earth Planet. Sci.*, *36*, 461–491.

McNutt, S. R., and T. Nishimura (2008), Volcanic tremor during eruptions: Temporal characteristics, scaling and constraints on conduit size and processes, *J. Volcanol. Geotherm. Res.*, *178*, 10–18.

Miyagi, Y., J. T. Freymueller, F. Kimata, T. Sato, and D. Mann (2004), Surface deformation caused by shallow magmatic activity at Okmok Volcano, Alaska, detected by GPS campaigns 2000–2002, *Earth Planet. Space*, *56*, 29–32.

Muyzert, E., and R. Snieder (1996), The influence of errors in source parameters on phase velocity measurements of surface waves, *Bull. Seismol. Soc. Am.*, *86*, 1863–1872.

Poupinet, G., W. L. Ellsworth, and J. Frechet (1984), Monitoring velocity variations in the crust using earthquake doublets: An application to the Calaveras fault, California, *J. Geophys. Res.*, *89*(B7), 5719–5731, doi:10.1029/JB089iB07p05719.

Ratdomopurbo, A., and G. Poupinet (1995), Monitoring a temporal change of seismic velocity in a volcano: Application to the 1992 eruption of Mt. Merapi (Indonesia), *Geophys. Res. Lett.*, *22*(7), 775–778, doi:10.1029/95GL00302.

Richter, C. F. (1943), Calculation of small distances, *Bull. Seismol. Soc. Am.*, *33*, 243–250.

Roberts, P. M., W. S. Phillips, and M. C. Fehler (1992), Development of the active doublet method for measuring small velocity changes and attenuation in solids, *J. Acoust. Soc. Am.*, *91*, 3291–3302.

Rowe, C. A., R. C. Aster, W. S. Phillips, R. H. Jones, B. Borchers, and M. C. Fehler (2002), Using automated, high-precision repicking to improve delineation of microseismic structures at the Soultz Geothermal Reservoir, *Pure Appl. Geophys.*, *159*, 563–596.

Sabra, K. G., P. Roux, P. Gerstoft, W. A. Kuperman, and M. C. Fehler (2006), Extracting coherent coda arrivals from cross correlations of long period seismic waves during the Mount St. Helens 2004 eruption, *Geophys. Res. Lett.*, *33*, L06313, doi:10.1029/2005GL025563.

Shapiro, N. M., M. H. Ritzwoller, and G. D. Bensen (2006), Source location of the 26 sec microseism from cross correlations of ambient seismic noise, *Geophys. Res. Lett.*, *33*, L18310, doi:10.1029/2006GL027010.

Snieder, R. (2006), The theory of coda wave interferometry, *Pure Appl. Geophys.*, *163*, 455–473.

Snieder, R., and M. Hagerty (2004), Monitoring change in volcanic interiors using coda wave interferometry: Application to Arenal Volcano, Costa Rica, *Geophys. Res. Lett.*, *31*, L09608, doi:10.1029/2004GL019670.

Snieder, R., A. Grêt, H. Douma, and J. Scales (2002), Coda wave interferometry for estimating nonlinear behavior in seismic velocity, *Science*, *295*(5563), 2253–2255.

Takagi, N., S. Kaneshima, H. Kawakatsu, M. Yamamoto, Y. Sudo, T. Ohkura, S. Yoshikawa, and T. Mori (2006), Apparent migration of tremor source synchronized with the change in the tremor amplitude observed at Aso volcano, Japan, *J. Volcanol. Geotherm. Res.*, *154*, 181–200.

Wegler, U., and D. Seidl (1997), Kinematic parameters of the tremor wave field at Mt Etna (Sicily), *Geophys. Res. Lett.*, *24*(7), 759–762, doi:10.1029/97GL00673.

Wegler, U., B.-G. Lühr, R. Snieder, and A. Ratdomopurbo (2006), Increase of shear wave velocity before the 1998 eruption of Merapi volcano (Indonesia), *Geophys. Res. Lett.*, *33*, L09303, doi:10.1029/2006GL025928.

Yamamoto, M., H. Kawakatsu, S. Kaneshima, T. Mori, T. Tsutsui, Y. Sudo, and Y. Morita (1999), Detection of a crack-like conduit beneath the active crater at Aso volcano, Japan, *Geophys. Res. Lett.*, *26*(24), 3677–3680, doi:10.1029/1999GL005395.

Yamamoto, M., H. Kawakatsu, K. Yomogida, and J. Koyama (2002), Long-period (12 sec) volcanic tremor observed at Usu 2000 eruption: Seismological detection of a deep magma plumbing system, *Geophys. Res. Lett.*, *29*(9), 1329, doi:10.1029/2001GL013996.

M. M. Haney, Department of Geosciences, Boise State University, 1910 University Dr., Boise, ID 83725, USA. (matt@cgiss.boisestate.edu)